Evidence against a role of elevated intracellular Ca^{2+} during *Plasmodium falciparum* pre-invasion

V. Introini, A.J. Crick, T. Tiffert, J. Kotar, Y.-C. Lin, P. Cicuta, V.L. Lew

Abstract

Severe malaria is primarily caused by *Plasmodium falciparum* parasites during their asexual reproduction cycle within red blood cells. One of the least understood stages in this cycle is the brief pre-invasion period during which merozoite-red cell contacts lead to apical alignment of the merozoite in readiness for penetration, a stage of major relevance in the control of invasion efficiency. Red blood cell deformations associated with this process were suggested to be active plasma membrane responses mediated by transients of elevated intracellular calcium. Few studies have addressed this hypothesis due to technical challenges, and the results remained inconclusive. Here, Fluo-4 was used as a fluorescent calcium indicator with optimized protocols to investigate the distribution of the dye in red blood cell populations used as *falciparum* invasion targets in egress-invasion assays. Pre-invasion dynamics was observed simultaneously under bright-field and fluorescence microscopy by recording egress-invasion events. All the egress-invasion sequences showed red blood cell deformations of varied intensities during the pre-invasion period and the echinocytic changes that follow during invasion. Intra-erythrocytic calcium signals were absent throughout this interval in over half the records, and totally absent during the pre-invasion period regardless of deformation strength. When present, calcium signals were of a punctate modality, initiated within merozoites already poised for invasion. These results argue against a role of elevated intracellular calcium during the pre-invasion stage. We suggest an alternative mechanism of merozoite-induced pre-invasion deformations based on passive red cell responses to transient agonist-receptor interactions associated with the formation of adhesive coat filaments.

1 Introduction

Most cases of severe malaria in humans are caused by the malaria parasite *Plasmodium falciparum* (*Pf*), one of the five malaria parasite species infecting humans. It is the asexual reproduction cycle of the parasite within human red blood cells (RBCs), initiated by merozoite invasion, that is responsible for the symptoms in malaria disease. *Pf* merozoites are pear-shaped spheroids of about 1.0-1.2 μm in diameter, with an apex structure that has to become aligned perpendicular to the RBC membrane for initiating parasite penetration (1, 2).

In studies of *Pf* growth using cultures sustained with RBCs of different densities, reflecting different hydration states, it was found that the invasion efficiency decreased progressively with the increase in RBC density (3). Because disease severity is associated with high parasitaemia, the density effect contributes protection by preventing the development of high parasitaemia in all inherited RBCs abnormalities associated with the presence of dense RBC subpopulations (3). The search for clues on possible mechanisms of this density effect focused attention on the events taking place between the instant a merozoite makes first contact with a RBC and the time when it becomes apically aligned, ready for invasion, the pre-invasion stage.

The pre-invasion stage is very brief, variably reported as lasting between 2 and 50 s (4–6). Microscopy, electron microscopy (7) and video-microscopy (4, 6, 8, 9) records of pre-invasion and invasion stages have collectively documented the following sequence of dynamic events during most of the pre-invasion periods observed so far: i) random initial merozoite-RBC contacts away from the merozoite apex elicit reversible interactions between merozoite coat agonists and RBC membrane receptors (1) with coat filaments of 20 to 150 nm length joining the two surfaces (7), ii) dynamic RBC deformations of variable intensity emanating from merozoite contact points, iii) a positional progression of the merozoite towards an irreversible apical contact driven by a gradient of increasing adhesin concentrations on the merozoite coat (10–12), iv) cessation of RBC deformations with restoration of normal biconcave shape (4, 8), and v) apex alignment of the irreversibly attached merozoite perpendicular to the RBC surface with formation of a tight junction structure (1, 4, 8, 13, 14). Merozoite penetration is frequently, but not always, accompanied by echinocytic shape changes of variable duration, usually about 5 to 15 minutes, after which the invaded cell regains its pre-invasion shape with a ring-shaped parasite within (4, 6). The membrane area

0006-3495/08/09/2624/12 $2.00 doi:

and volume of host RBCs was shown to remain essentially unchanged during all these shape changes (15, 16).

The pre-invasion period remains one of the least understood stages of the malaria invasion process. Much progress has been made on the molecular and genetic identity of the variety of agonist families on the merozoite coat and of the receptors on the RBC surface that mediate the reversible and irreversible interactions operating during pre-invasion and invasion stages (1, 12, 17–19). This contrasts with the meager progress made in the understanding of the mechanistic dynamics at play during pre-invasion.

The only working hypothesis advanced so far on the mechanism of the merozoite-induced RBC deformations involves calcium mediation (5). The hypothesis was based on two critical assumptions: i) that the merozoite-elicited RBC deformations were an active response of the RBC membrane aimed at speeding up apical contacts (4) thus increasing invasion efficiency, a response progressively inhibited in dense RBCs; and ii) that the deformations were caused by transients of local intracellular calcium concentration ($[Ca^{2+}]_i$) increase at the inner membrane surface, based on evidence that invasion was strongly dependent of the presence of calcium in the medium (10, 20–22).

Weiss *et al.* (10) carried out a thorough investigation of the role of calcium during pre-invasion and invasion stages by adding purified schizonts to RBCs loaded with the calcium-sensitive fluorescent dye Fluo-4. In 248 invasion events recorded on alternating lapse-time sequences under bright-field and fluorescence, Ca^{2+}signals were detected only in 45% of instances. When present, the Ca^{2+}signals appeared towards the end of deformations and displayed a characteristic sequence starting with an intense punctate signal localized to the merozoite, followed by a variable diffusion pattern within invaded RBCs undergoing echinocytic transients (10).

At face value, these results suggest that $[Ca^{2+}]_i$ elevations play no role in the dynamic deformations assumed necessary for apical alignment, against the tenets of the calcium hypothesis. However, a number of technical and methodological issues prompted the need for a reassessment of the evidence and for further research to resolve the role of $[Ca^{2+}]_i$ during pre-invasion, penetration and immediate post-invasion stages. We consider these issues next.

A main methodological concern applies to the correct use of Fluo-4 in the conditions of merozoite invasion tests. Fluo-4 is loaded into cells with the use of its acetoxymethyl derivative, Fluo-4 AM, but AM derivatives do not permeate membranes. The hydrophobicity of the X-AM complexes allows them to rapidly partition into the hydrophobic core of cell lipid bilayers when added dissolved in dimethyl sulfoxide (DMSO) into cell suspensions. From there, esterases operating at the inner membrane surface break down the AM residues releasing free X into the cell cytoplasm. In their original work, Tsien *et al.* (23–27) assumed that the formaldehyde released as a byproduct of AM hydrolysis diffused away from the cells with no toxic side-effects. But Tiffert *et al.* (28), showed that all the formaldehyde released remains retained within the cells, and that for cells that depend on glycolytic metabolism for ATP synthesis, such as RBCs, formaldehyde exerts a powerful metabolic block on glycolytic ATP production. In substrate-free media, formaldehyde has no effect on the ATP content of the cells (28). In the presence of glucose, X-AM or formaldehyde treatments cause a sharp fall in cell ATP (28). This happens because ATP is rapidly consumed by hexokinase-mediated phosphorylation during the initial steps of glycolytic metabolism while downstream ATP synthesis is blocked.

The formaldehyde-induced glycolytic block can be easily prevented by the inclusion of pyruvate in incubation or culture media (29, 30). In the experiments of Weiss *et al.* (10), Fluo-4 AM exposure was in glucose-containing RPMI, without pyruvate. Therefore, target RBCs may have been depleted of ATP, a necessary cofactor for invasion (31) rendering the assumed normality of the reported invasion responses questionable.

Additional issues of concern in the experiments of Weiss *et al.* (10) relate to the possibility of false negative Ca^{2+}signals from cells with low Fluo-4 loads, and of relatively prolonged time-gaps in lapse-time records, missing fleeting, and potentially relevant events. The distribution of Fluo-4 in the RBC population was not investigated leaving open the possibility that Ca^{2+}signals from low-Fluo-4 RBCs were below detectable levels. In the sample of lapse-time images, alternating bright-field and fluorescence images, critical periods of observation were missing. Records with higher time resolution are clearly needed to convincingly rule out transient Ca^{2+}signals during pre-invasion. In the experiments reported here we address each of these issues in detail.

2 Materials and Methods

2.1 Chemicals and solutions

The experiments were performed using the following solutions referenced in the text. All chemicals were obtained from Sigma-Aldrich (Gillingham, UK), if not otherwise specified. Solution A: NaCl, 145 mM; KCl, 3 mM; Na-HEPES (pH 7.5 at 37 °C), 10 mM; $MgCl_2$, 0.15 mM. Solution AE: as A plus Na-EGTA, 0.1 mM. Solution AIP: as A plus inosine, 5 mM; Na-pyruvate, 5 mM. Solution HKIP: NaCl, 60 mM; KCl, 90 mM; Na-HEPES (pH 7.5 at 37 °C), 10 mM; $MgCl_2$, 0.15 mM; $CaCl_2$, 0.20 mM; inosine, 5 mM; Na-pyruvate, 5 mM. Wash medium (WM): RPMI-1640 supplemented with HEPES, 40 mM; D-glucose, 10 mM; glutamine, 2 mM; and gentamicin sulphate, 25 mg/L. Wash medium with pyruvate (WMP): as WM with Na-pyruvate,

5 mM. Culture medium (CM): as WM plus AlbumaxII, 0.5% vol/vol. Culture medium with pyruvate (CMP): as CM plus Na-pyruvate, 5 mM.

2.2 Malaria culture

Pf A4 (32) and 3D7 parasites were cultured in human RBCs from healthy volunteers under low-oxygen atmosphere (1% O_2, 3% CO_2, 96% N_2) according to standard protocols (33–35); the culture medium was changed daily. The RBCs were isolated from leucocytes and platelets using Lymphoprep (STEMCELL Technologies, Cambridge, UK) and used within 7 days. *Pf* cultures were synchronized by the sorbitol lysis method (36) as needed; mature trophozoies and schizonts were selected from cultures by gelatine flotation (27, 28, 37, 38) or by magnetic separation (39). Parasitaemia was assessed by microscopic inspection of Giemsa-stain blood smears (40).

2.3 Incorporation of Fluo-4 in RBCs

Fluo-4 was incorporated non-disruptively into RBCs using the acetoxymethyl derivative Fluo-4 AM (Invitrogen Ltd., Paisley, UK). The stock solution of Fluo-4 AM in DMSO was prepared to a concentration of 0.5 mM. Fresh RBCs were washed twice in AE, once more in AIP, and resuspended in AIP at 10% Hct. Fluo-4 AM in DMSO was added to the cell suspension to provide a final concentration of 5 μM. The suspension was incubated at 37 °C for 45 minutes, washed twice in WMP, and finally suspended in CMP. The suspension was incubated for a further 15 minutes to enable the complete de-esterification of the Fluo-4 AM molecules, as suggested in the product manual. The entire Fluo-4 loading procedure was performed under minimal light exposure.

2.4 Formaldehyde loading of RBCs

Fresh RBCs were washed and suspended at 10% Hct in solution A with no metabolic substrates. Formaldehyde was added from a 1 M stock solution to half of the RBC suspension to a final concentration of 0.4 mM, and both suspensions were incubated at 37 °C for 1 h. After the incubation time, RBCs from each suspension were washed twice in A, resuspended in CM at 2% Hct and distributed in two flasks. Four different suspensions were obtained: control (C), control + pyruvate (C + Pyr), formaldehyde (FA), and formaldehyde + pyruvate (FA + Pyr). For the experiments, an aliquot of *Pf* A4 clone suspension (32) with about 80% parasitaemia of mature trophozoites and schizonts was added to each flask to obtain an initial parasitaemia of around 3%. This was followed by incubation of the flasks at 37 °C under low O_2 for about 28 h, at which time parasitaemia was assessed by inspection of Giemsa-stained culture smears. Parasitaemias were measured by counting 2000 RBCs in triplicates, with replicate percentages agreeing within 5%. The results are reported and analysed in Section 3.1 and Fig. 1a.

2.5 Parasite culture in Fluo-4-loaded RBCs with pyruvate

Fresh RBCs, suspended in WM at 2% Hct were loaded with Fluo-4 by adding Fluo-4 AM to a final concentration of 10 μM in the suspension (10). In these conditions, full Fluo-4 incorporation into the small 2% fraction of RBCs would generate a Fluo-4 concentration of 0.5 mmol/L cells. With a stoichiometry of four molecules of formaldehyde released per molecule of Fluo-4 incorporated, the concentration of formaldehyde experienced by the cells would be about 2 mmol/L cells. Half of the cells were resuspended in WM and half in WMP, incubated at 37 °C for 1 h and washed 3 times in 10 volumes of WM (10). Finally, the cells were loaded in chambers labelled as Fluo-4 and Fluo-4 + pyruvate (Fluo-4 + Pyr). Enriched 3D7 strain schizonts isolated by magnetic separation were added to both cultures and to a control sample of untreated RBCs (RBCs without Fluo-4 at 2% Hct) to obtain an initial parasitaemia of 3%. Parasitaemias in Fig. 1b were estimated after 28 h from 4 experiments, and p-values were calcualted using an unpaired t test.

2.6 Ionomycin-treated RBCs

Fluo-4-loaded RBCs as described in Section 2.3 were washed twice and resuspended at 10% Hct in HKIP. Ionomycin stock solution in DMSO (2 mM) was added to a final concentration of 0.2 μM. The entire procedure was performed at room temperature.

2.7 Vanadate-treated RBCs in low-K^+ and high-K^+ media

1 mL of RBCs was loaded with Fluo-4 in AIP as described in Section 2.3. A 0.1 mL aliquot was used as a control and to the remaining 0.9 mL vanadate and $CaCl_2$ were added to render final concentrations of 1 mM each, from stock solutions of vanadate (100 mM) and $CaCl_2$ (200 mM).

A similar protocol was applied for vanadate-treated RBCs in high-K^+ medium: Fluo-4-loaded RBCs were washed twice and resuspend in HKIP at 10% Hct. Vanadate was added to the suspension to a concentration of 1 mM. Samples from control and vanadate-treated suspensions in low-K^+ and high-K^+ media were loaded in chambers for observation.

2.8 Imaging of the calcium egress-invasion assay

A 3D7 *Pf* suspension at 0.2% Hct with at least 80% parasitaemia was prepared for imaging by mixing Fluo-4-loaded uninfected RBC (see Section 2.3) with an aliquot of

highly concentrated (97-100%) parasitized RBCs obtained by magnetic separation. Imaging was done in SecureSeal Hybridization Chambers (Sigma-Aldrich). A custom-built temperature-control system was used to maintain the optimal culture temperature of 37 °C during imaging experiments. The sample was placed in contact with a transparent glass heater driven by a PID temperature controller in a feedback loop with the thermocouple attached to the glass slide. A Nikon Eclipse Ti-E inverted microscope (Tokyo, Japan) was used with a Nikon 60X Plan Apo VC, NA 1.40, oil-immersion objective, kept at 37 °C through a heated collar. Motorized functions of the microscope were controlled via custom software written in-house. Images were acquired using a CMOS camera (model GS3-U3-23S6M-C, Point Grey Research/FLIR Integrated Imaging Solutions (Machine Vision), Ri Inc., Canada). Focus was maintained throughout experiments using Nikon Perfect Focus hardware.

In order to record invasion events in bright-field and Ca^{2+}signals under fluorescence, with high time resolution, the microscope was equipped with a custom-built light-emitting diode (LED)-based illumination system. The system allows synchronizing camera frames with different LEDs (Mouser Electronics, High Wycombe, UK) of the illumination system with a predefined camera driven sequence. We used an alternating sequence of green LED (LED Engin LZ4-24MDCA-0000, 523nm peak wavelength) for bright-field illumination and blue LED (Lumileds LXZ1-PB01, 470nm peak wavelength) for epi-fluorescence illumination with fluorescence filter block (Semrock GFP-3035D, exciter FF01-472/30, dichroic FF495-Di03, emitter FF01-520/35; Rochester, New York, USA). In recorded events, frames were acquired in bright-field and fluorescence in an alternating fashion with an exposure time of 200 ms.

We found that recording events at 5 frames per second (fps) optimized the fluorescent signal from invaded cells loaded with Fluo-4 while providing a detailed resolution of the pre-invasion and invasion process. Each experiment lasted about 2 h to enable recording of a sufficient number of events and was performed in darkness to prevent photobleaching and to avoid signals from the environment.

3 Results

3.1 Effects of formaldehyde and pyruvate on Plasmodium falciparum invasion and growth

The aim of these experiments was to establish whether *Pf* invasion could be affected by the formaldehyde released during the incorporation of AM-compounds into RBCs, and, if so, whether pyruvate could prevent these effects (41). Fluo-4 AM was added to RBC suspensions to generate a final concentration of 1-2 mmol/L cells of Fluo-4, assuming full release of the free dye into the cell (6, 28, 41). The concentration of formaldehyde released and trapped by the cells after Fluo-4 loading reached 4 to 8 mmol/L cells on full ester hydrolysis (28), and 4 mmol/L cells was the concentration tested in the experiments of Fig. 1a following the protocol in Section 2.4.

During the growth assay in glucose-containing RPMI medium, ATP was expected to fall rapidly in formaldehyde-treated cells, but only in the absence of pyruvate. Merozoites released during the first hours of incubation would thus encounter different ATP contents in RBCs under formaldehyde and formaldehyde + pyruvate conditions. Under test was the comparison of growth in these two conditions. The results (Fig. 1a) showed that parasite growth was comparable in controls and in formaldehyde-treated cells in the presence of pyruvate (Fig. 1a: C, C + Pyr, and FA + Pyr). Growth was almost fully inhibited in the culture with formaldehyde-treated cells in the absence of pyruvate (Fig. 1a: FA). The near total absence of iRBCs or of Giemsa-stained residual parasite material in this condition suggested that invasion was minimally consummated in these cells. The fact that pyruvate fully prevented this effect indicated that ATP must have been depleted to levels incompatible with invasion in the formaldehyde-treated cells by the time most merozoites had egressed. These results support the early conclusions of Dluzewski *et al.* (31), based on experiments with resealed ghosts, that ATP depletion prevents invasion.

To evaluate the extent to which the formaldehyde effects reflected those caused by Fluo-4 incorporation when using the experimental protocol of Weiss *et al.* (10), we investigated the effects of pyruvate on growth by replicating their experimental conditions (see Section 2.5). We compared growth in RBCs loaded with Fluo-4 in the presence or absence of pyruvate and the results are shown in Fig. 1b. In the absence of pyruvate (Fig. 1b: Fluo-4), growth was reduced by about 30% relative to Fluo-4-free control and Fluo-4 + pyruvate (Fig. 1b: C, Fluo-4 + Pyr), confirming that the invasion efficiency was reduced in ATP-depleted RBCs. Once invasion occurs, no difference was noticed in the development of the parasites at ring stage between Fluo-4 and Fluo-4 + pyruvate conditions.

When comparing the results in Figs. 1a and 1b, it is important to note that with the protocol in Fig. 1a formaldehyde was delivered instantly and uniformly to all the cells at the maximal intended concentration, whereas with the protocol of Weiss *et al.* (10) in Fig. 1b, formaldehyde would have been released more slowly, at the rate of AM-ester breakdown in each cell during Fluo-4 incorporation. Moreover, as documented below in Figs. 3 and 5, Fluo-4 loads varied substantially among the cells and hence also the extent of formaldehyde trapped by each cell, causing variable rates and extents of ATP depletion in the RBC population. Thus, the limited growth inhibition observed with the protocol of Weiss *et al.* (10) relative to that of Fig. 1a could be explained by the slower and reduced formaldehyde release from cell subpopulations with varied esterase activity incorporating submaximal levels of Fluo-4 (Fig. 3).

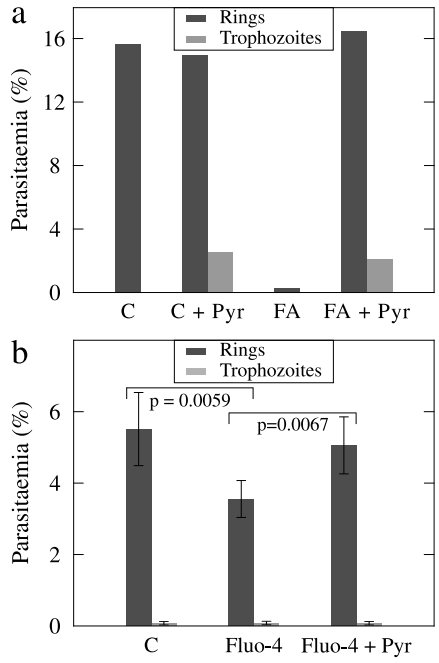

Figure 1: Effects of formaldehyde and Fluo-4-AM on *Pf* invasion in the presence or absence of pyruvate. (a) RBCs were exposed to formaldehyde in the absence (FA) or presence of pyruvate (FA + Pyr) as detailed in 2.4. The results were compared with formaldehyde-free controls in the absence (C) or presence of pyruvate (C + Pyr). *Pf* A4 clone parasitaemias were measured after 28 h, and triplicates agreed within 5%. (b) Effects of Fluo-4 loading following the experimental protocol of Weiss *et al.* (10), as reported in 2.5. *Pf* 3D7 parasitaemias of 4 experiments were measured after 28 h culture in controls not exposed to Fluo-4-AM (C), and in Fluo-4-AM treated RBCs in the absence (Fluo-4) and presence of pyruvate (Fluo-4 + Pyr). Significant differences ($p<0.05$) are shown in the graph.

3.2 Distribution of Fluo-4 in treated RBCs

To ascertain the reliability of Fluo-4-loaded RBCs to report Ca^{2+}signals in invasion assays avoiding false negatives, it was necessary to investigate the population distribution of the fluorescent Ca^{2+}dye and confirm that all cells contained enough dye to generate detectable signals. In physiological conditions RBCs maintain $[Ca^{2+}]_i$ of about 10-50 nM by a balance between inward Ca^{2+}leak (P_{Ca}) and active Ca^{2+}extrusion via the ATP-fuelled plasma membrane calcium pump (PMCA) (Fig. 2) (42). The physiological pump-leak turnover rate varies within the range of 10 to 50 μmol/(L cells·h), depending on cell age and medium conditions (26, 43, 44). The K_d of Fluo-4 for $Ca^{2+}$is about 345 nM, so that fluorescent signals are expected to become detectable in RBCs containing sufficient dye when $[Ca^{2+}]_i$ increases above 80-100 nM (45).

In the current study we used ionomycin, a non-fluorescent Ca^{2+}ionophore, and vanadate, a cell permeant, irreversible inhibitor of ATP-fuelled pumps, to elevate $[Ca^{2+}]_i$ and thus elicit Fluo-4 fluorescent signals (46, 47).

The interplay of these agents with the transport systems relevant to RBC Ca^{2+}homeostasis is illustrated in Fig. 2. With ionomycin, it is possible to increase the Ca^{2+}permeability of the plasma membrane to levels exceeding the maximal Ca^{2+}extrusion capacity of the PMCA, generating a uniform high-Ca^{2+}load in all the cells of a given sample, thus saturating the Fluo-4 light-emission intensity from every cell in the population. In these conditions, variations in the fluorescence signal report the true distribution of incorporated Fluo-4 in the RBC population. With vanadate, the intensity distribution of the generated fluorescent signals is a composite of the distributions of Fluo-4 and of the physiological Ca^{2+}permeability (P_{Ca}) in the RBC population (28, 48). Fluorescence intensity distributions may be explored with the RBCs suspended in low-K^+(plasma-like) or high-K^+media. In low-K^+media, activation of the Ca^{2+}-sensitive K^+channels of RBCs (49–51) hyperpolarizes the cells and causes the net loss of KCl and water (Fig. 2). This leads to cell dehydration and shrinkage, easily detectable under bright-field observation, offering a Fluo-4 independent visual estimate of the distribution of $[Ca^{2+}]_i$ when high enough to activate the Gardos channels ($[Ca^{2+}]_i > 70$-80 nM) (44, 52)). A comparative analysis of the fluorescence distributions and of the dehydration response elicited by ionomycin and vanadate was expected to allow a rough estimate of the stochastic probability of invasion events in Fluo-4-loaded RBCs failing to produce detectable fluorescent signals (false negatives).

Representative bright-field and fluorescence images of Fluo-4-loaded RBCs exposed to ionomycin or vanadate are shown in Figs. 3 and 4, respectively. Under bright-field, the control is largely dominated by normal-looking biconcave cells; using fluorescence, no signal is detected from any of the RBCs in the corresponding field (Fig. 3). The isolated strong signals visible at higher magnifications in the corresponding inset in bright-field (Fig. 3) can be attributed to the tiny proportion (<0.1%) of contaminant lymphocytes retained in isolated RBC preparations.

Ionomycin-treated RBCs, suspended in low-K^+medium for observation, appear uniformly shrunken in bright-field (Fig. 3) as expected with RBCs in dehydrated conditions with uniform Ca^{2+}-saturation of their Gardos channels. The distribution of fluorescence intensities in the ionomycin-treated cells (Fig. 3) show a wide variation, reflecting the actual Fluo-4 distribution in the RBC population. A careful comparison with the corresponding bright-field image shows Ca^{2+}signals emanating from all the cells. Thus, despite the large variation in Fluo-4 contents, all the cells in the population generate detectable Ca^{2+}signals at Fluo-4-saturating $[Ca^{2+}]_i$ levels.

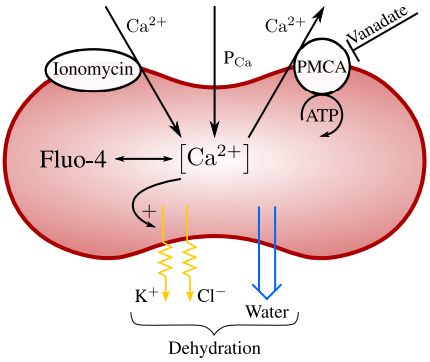

Figure 2: Illustration of the effects of ionomycin and vanadate on the calcium homeostasis of human RBCs. In physiological conditions, Ca^{2+}ions enter RBCs through low-permeability pathways (P_{Ca}) and are extruded by the ATP-fuelled plasma membrane Ca^{2+}pump (PMCA). Free Fluo-4 binds to Ca^{2+}ions with a K_d around 345 nM generating a fluorescent signal (45). Physiological $[Ca^{2+}]_i$ levels ($\leq$ 50 nM) remain below the detectable threshold. Increasing the Ca^{2+}permeability with ionomycin or inhibiting the PMCA with vanadate elevates $[Ca^{2+}]_i$, enhancing the fluorescence signal. Elevated $[Ca^{2+}]_i$ activates Ca^{2+}-sensitive K^+-channels in the RBC plasma membrane leading to KCl and water loss with cell dehydration and shrinkage.

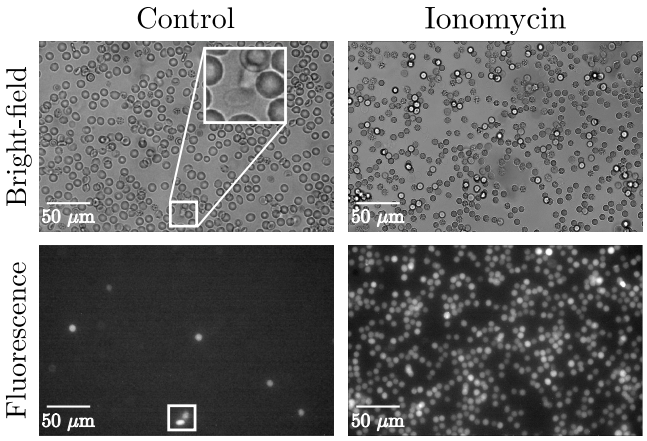

Figure 3: Effects of ionomycin-induced calcium loads on the bright-field appearance and fluorescence signal from Fluo-4-loaded RBCs. Results representative of four similar experiments. Note the dominant normal biconcave discocyte appearance of the control RBCs (top left panel), and the lack of fluorescent signal (bottom left panel). The isolated intense fluorescent spots do not relate to intact RBCs, as illustrated for one such spot in the inset. The dominant appearance of the ionomycin-treated RBCs is that of profoundly shrunken and crenated RBCs (top right panel). Individual fluorescent signals (bottom right panel) can be traced to each corresponding cell in the bright field image (top right panel). Thus, at saturating Ca^{2+}loads the presence of Fluo-4 is revealed in all cells, but the cell-load distribution appears substantially uneven.

Bright-field images of vanadate-treated cells (Fig. 4) show typical fields of dehydrated, shrunken cells in low-K^+medium, and of non-dehydrated cells with largely preserved discocyte shapes in high-K^+medium. In fluorescence (Fig. 4), Ca^{2+}signals are detected in the majority, but not in all, of the cells of the corresponding bright-fields. This is particularly noteworthy for the cells suspended in high-K^+medium. Compared with ionomycin-treated cells (Fig. 3), vanadate-treated cells show overall reduced fluorescence levels and sharper cell-to-cell differences, reflecting wider variations in Ca^{2+}gain. The distribution of fluorescent intensities assessed 3 h later showed no significant difference, suggesting that the intracellular calcium concentration had already reached saturation levels for the Fluo-4 signal in most cells. The shown intensity distribution approximates best the true fluorophore distribution in the RBC population. $[Ca^{2+}]_i$ levels appear higher in cells suspended in low-K^+than in high-K^+media (Fig. 4) for two reasons. Firstly, cell shrinkage in low-K^+conditions increases $[Ca^{2+}]_i$ at comparable total calcium concentrations. Secondly, a substantial component of the Ca^{2+}leak (P_{Ca}, Fig. 2) is electrodiffusional. The hyperpolarization generated by Gardos channel activation in low-K^+media increases the driving gradient for Ca^{2+}influx tending to elevate $[Ca^{2+}]_i$.

The fluorescence distributions obtained in these different conditions are quantified in the histograms of Fig. 5.The images in Figs. 3 and 4 were segmented into regions that identified every single cell in bright-field, and partial cells at the edges were excluded using a mask. This segmentation was then superimposed on the fluorescence image of the same field of view, and after background subtraction the average intensity of the pixels within each cell was measured, to construct an intensity distribution across cells (Fig. 5). The fluorescence intensity distributions for ionomycin- and vanadate-treated RBCs are significantly above background for the vast majority of the cells. The distribution of Fluo-4 in ionomycin-treated cells is very broad, with a standard deviation of 31% of the mean, considerably higher than the 20% previously recorded for fura-2 incorporation (53). The distributions of fluorescence intensities in vanadate-treated cells are much narrower, with substantially lower means, reflecting permeability-restricted Ca^{2+}influx, more severe in the high-K^+condition in which around 3% of the cells are below the background.

Ca^{2+}signals were detected from most of the vanadate-treated shrunken cells suspended in low-K^+medium (Fig. 4). The mean physiological $[Ca^{2+}]_i$ level within human RBCs suspended in plasma is about 50 nM (26). In the absence of precise in situ calibrations of the Fluo-4 signal, the Fluo-4 detection level for $[Ca^{2+}]_i$ remains unknown. It is therefore

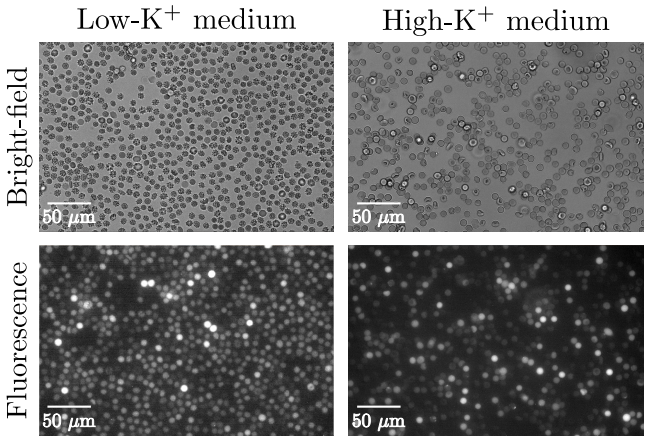

Figure 4: Effects of vanadate-induced PMCA inhibition on the bright-field appearance and fluorescence signal from Fluo-4-loaded RBCs in low-K^+ and high-K^+media. Results representative of six similar experiments. The resulting fluorescence distributions are a composite of true variations in Fluo-4 contents and differences among cells in calcium leak (P_{Ca}). In low-K^+media the dominant appearance is that of dehydrated RBCs (top left panel), contrasting with the dominant normal discocyte appearance of the cells in high-K^+media (top right panel), where dehydration is prevented. Fluorescence intensities (bottom panels) vary sharply among the cells, with no signal at all from a substantial fraction of cells in both conditions.

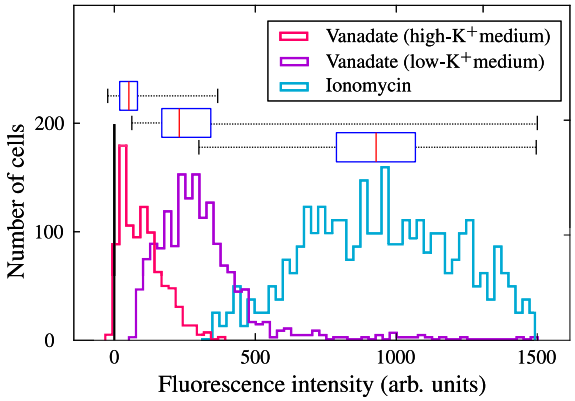

Figure 5: Distributions of fluorescence signal intensities from Fluo-4 loaded RBCs treated with ionomycin or vanadate. Mean background signal intensity was estimated from the controls, and it was set as the x-axis zero. The total fluorescence was calculated by subtracting the background mean from each individual cell's intensity. Fluorescence intensity from low-K^+vanadate and ionomycin distributions is distinctively higher than the control (RBCs with Fluo-4 only). In the high-K^+condition, the fluorescence intensity is lower than in the low-K^+condition, reflecting a permeability-restricted Ca^{2+}influx. In the box plots, the red line indicates the median, the box indicates the 25^{th} and 75^{th} percentiles of the samples, and whiskers denote total data range.

important to note that $[Ca^{2+}]_i$ elevations between physiological levels and Fluo-4 threshold would remain undetected. However, there is strong evidence that the Ca^{2+}-sensitive Gardos channels of the RBC membrane (Kcnn4) (49, 54, 55) remain viable but inactive during invasion (56, 57). This offers an independent estimate of the top limit to which $[Ca^{2+}]_i$ may increase when undetected by Fluo-4. Based on early calibrations of the Ca^{2+}sensitivity of the Gardos channel in human RBCs (52, 58) this top limit is about 80-100 nM. Therefore, our results cannot rule out $[Ca^{2+}]_i$ increases below this limit during invasion.

3.3 Video microscopy recordings of egress-invasion sequences

We followed the invasion process in 20 Fluo-4-loaded RBCs, from merozoite egress to post-invasion echinocytosis, by video recording under bright-field and fluorescence at 5 fps (see Section 2.8). Ca^{2+}signals were not detected in 11 out of 20 experiments. Weiss-Gilson *et al.* (10) also reported about 55% negative results. However, the probability that this is due to undetectable signals from cells with poor Fluo-4 loads, given the Fluo-4 distributions shown in Figs. 3, 4, and 5, is vanishing small.

In all 9 cells with a positive fluorescent response, the fluorescent Ca^{2+}signals were fully confined to the post-alignment stages.

All Ca^{2+}signals detected were of the punctate modality described in detail by Weiss-Gilson *et al.* (10). Figure 6 shows selected frames of Video S1 (in Supportings Material), representative of a typical punctate response in which the intensity of the Ca^{2+}signal was high indicating provenance from cells with high Fluo-4 loads, recorded with higher time-resolution (10 fps). More than 2 s after the first deformation response to merozoite contact (shown on bright-field at 1.4 s post-egress) a peak of intense fluorescence, entirely localized to the body of the merozoite, appears within the 0.1 s transition from baseline fluorescence to the next video frame. The following frames show a gradual increase in fluorescence within the boundaries of the invaded RBC towards a homogeneous fluorescence distribution reached after about 5 s post-egress, as shown in Fig. 6. The changes in fluorescence intensity gradients clearly point to the merozoite as the main source of elevated RBC Ca^{2+}. In all 20 experiments of this series, no Ca^{2+}signal was seen to originate from locations other than the merozoite. In the 11 punctate-negative experiments, absence of Ca^{2+}signals included all echinocytic periods. These results suggested

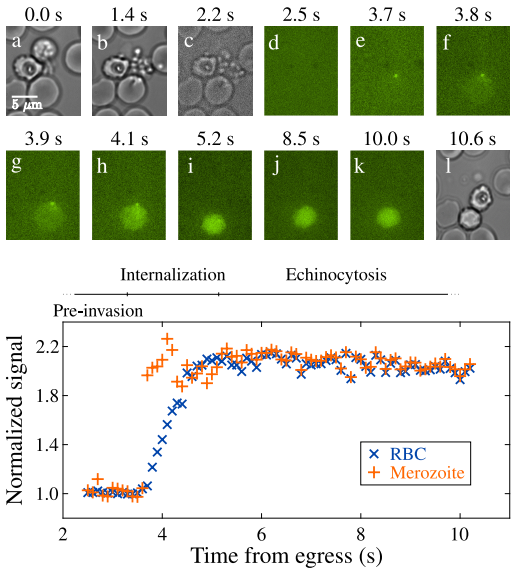

Figure 6: Video recording of an egress-invasion sequence in Fluo-4 loaded cells (Video S1) with a high fluorescent intensity punctate response. Selected snapshots are shown in the top panel; the bottom plot quantifies the changes in fluorescent intensities of merozoite and RBC regions over time, normalized to the surrounding background in each frame. **Snapshots**: (a-b) a merozoite upon contact with a healthy RBC triggers cell deformation at 1.4 s after egress; (c) switch from bright-field to fluorescence channel; (d) the first frame in fluorescence is recorded at 2.5 s but no fluorescence signal is visible until (e) a strong signal at 3.7 s is almost entirely confined to the merozoite area and appears as a Fluo-4 saturating intensity, 2.3 s after merozoite contact and local deformation in frame (b); (f-h) rapid diffusion of the fluorescent signal from the invading merozoite to the RBC in about 0.4 s; (i-k) merozoite fluorescence merges with the uniform RBC fluorescence, signaling parasite internalization; (l) echinocytic condition of invaded RBC at the end of recording, on return, to bright-field imaging. **Bottom Plot**: Time-sequence of merozoite and target-cell Ca^{2+}signals during a typical punctate response. It shows the absence of a Ca^{2+}signal during the pre-invasion period, and the extended duration of the high Ca^{2+}signal during the echinocytic stage.

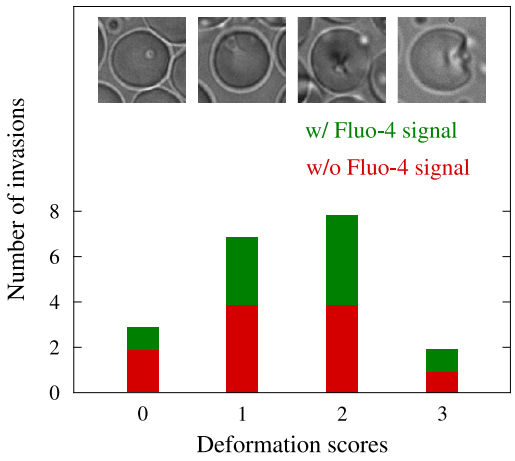

Figure 7: Scoring the deformation intensities associated with presence or absence of calcium signals during the twenty experiments of this series. Our scoring was derived from the original Weiss *et al.* (10) classification. Samples of the 0 to 3 scores used here are shown at the top. Note the absence of correlation between the deformation level and the presence (green) or absence (red) of Ca^{2+}signal.

no increase in the calcium permeability of the RBC membrane throughout invasion, and that elevated $[Ca^{2+}]_i$ was not required for echynocytosis.

An example of invasion processes in which RBCs show weak Ca^{2+}signals from low Fluo-4 loads is reported in Video S2 and in the analysis of Fig. S3 in the Supporting Material. No signal was detected during pre-invasion periods both in the case of high and low $[Ca^{2+}]_i$ (Figs. 6, S3 and Videos S1, S2) thus ruling out false negative results in this series. Taken together, these results made a strong case against the hypothesized role of calcium in pre-invasion deformations. Ca^{2+}signals were only detected as an episodic occurrence during post-alignment events.

In conclusion, the constant features in all the nine records with positive Ca^{2+}signals were the punctate response to merozoite alignment, and the sustained increase in Ca^{2+}signal intensity post-invasion. Variable, inconstant or uncertain features were i) the original $[Ca^{2+}]_i$ level within individual target cells (compare background signals in Videos S1 and S2), ii) the duration of the pre-invasion stage, iii) the presence and duration of post-invasion shape-quiescent periods, and iv), the delay and morphological progression to echinocytosis, from gradual to explosive.

3.4 Deformation response of RBCs to initial merozoite contacts

In the original formulation of the calcium hypothesis (5), deformations were assumed to be calcium-driven active RBC membrane responses required for apical alignment. In the absence of detectable calcium signals during the pre-invasion period, are deformations still active and relevant to merozoite alignment? Could deformation intensity still be correlated with late positive Ca^{2+}signals, potentially associated with subliminal $[Ca^{2+}]_i$ elevations during pre-invasion stages? Using the approach developed by Weiss *et al.* (10), we scored the pre-invasion deformations observed under bright-field in each of the twenty experiments of this series. The results in Fig. 7 showed no preferential correlation with presence (green) or absence (red) of Ca^{2+}signals at any of the deformation intensities scored.

4 Discussion

We investigated the hypothesized role of elevated $[Ca^{2+}]_i$ on the deformation responses that merozoite contacts elicit in RBCs during the pre-invasion period (5). We sought to overcome methodological uncertainties from earlier studies concerning the ATP depletion status of the RBCs targeted for invasion, the possibility of false negatives from low-Fluo-4 containing RBCs, and the possibility of brief events being missed during the relatively large gaps in early lapse-time video recordings (10). Ca^{2+}signals were recorded from Fluo-4-loaded RBCs in conditions which ensured preservation of their normal ATP contents (Fig. 1). The distribution of Fluo-4 in the RBC population was measured under a variety of conditions and found to vary widely, but all RBCs were shown to contain sufficient Fluo-4 to elicit detectable Ca^{2+}signals at saturating Ca^{2+}loads (Figs. 3, 4, and 5). Egress-invasion sequences were followed and video-recorded under bright-field and fluorescence in Fluo-4-loaded RBCs at frequencies of between 5 and 10 fps, a 10 to 15 fold improvement on the time-resolution of previous lapse-time recordings (Figs. 6, S3 and Videos S1, S2). Our results resolve lingering concerns and gaps from earlier studies (10), provide strong evidence against the calcium hypothesis (5), and offer a novel insight on the mechanics of merozoite-RBC interactions during the pre-invasion stage.

In the 20 egress-invasion assays reported here, Ca^{2+}signals were recorded only in 9 (Figs. 6, S3 and Videos S1, S2), all of the punctate modality originally described by Weiss *et al.* (10). Ca^{2+}signals were never detected during pre-invasion stages regardless of presence, absence or intensity of late fluorescent signal (Figs. 6, S3 and Videos S1, S2) or of the intensity of the deformation response (Fig. 7). Taken together, these results argue against the hypothesized role of $[Ca^{2+}]_i$ elevations on merozoite-elicited deformations (5)), unless confined to sub-membrane microdomains within levels below Gardos channel activation, undetectable by Fluo-4.

The conclusions concerning calcium agree with those of McCallum-Deighton and Holder (22) that the role for calcium in merozoite invasion is extracellular (10). Results of Gao *et al.* (59), demonstrate that calcium is required by merozoites for Ca^{2+}signaling of EBA-175 discharge leading to apical junction formation, and indicate that all merozoites poised for invasion are in a high Ca^{2+}signaling condition (19, 60). The interaction between PfRh5 and basigin was shown to be essential for establishing the tight junction between merozoite and host during invasion, an event associated with Fluo-4 signals of elevated Ca^{2+}in merozoite and host cells (61, 62). In the paper by Volz *et al.* (62), Ca^{2+}signals were detected in only 41 out of 178 merozoite contacts associated with host cell deformations, and 36 of the 41 progressed to invasion (62). The Ca^{2+}signal for 3D7 in their Fig. 5A shows the typical punctate response associated with events following irreversible apical alignment, hard to attribute to pre-invasion events. The paper by Aniweh *et al.* (61), provides elegant evidence for the essential role of the PfRh5-basigin interaction in merozoite invasion. But the implicit assumption that the elevated Ca^{2+}signals they detected for the post-alignment period occur in all invasion instances is not supported by their evidence, which was based on population signals from a fluorescence plate reader, or by isolated observations on single invasion events. The episodic occurrence of post-alignment Ca^{2+}signals reported in our casuistic and in that of Weiss *et al.* (2015) (10) may result from i) stochastic permeability pathway configurations affecting diffusional patterns for Ca^{2+} and Fluo-4 between merozoite and host, ii) a Ca^{2+}signal required for successful invasion of age-discriminated target RBCs, or iii), false negatives due to poor documentation of successful invasion among some of the Ca^{2+}-negative results.

4.1 On the possible function of punctate responses

With this in mind, the lack of Ca^{2+}signals in 55% of invasions recorded in Fluo-4-loaded RBCs could only have resulted from the lack of free Fluo-4 access to Ca^{2+}-activated merozoites. Other than presence or absence of Ca^{2+}signals there were no alternative features that could help distinguish the dynamics of pre-invasion and invasion patterns between the two groups. Free Fluo-4 was present initially only within the RBC cytoplasm (Figs. 3 and 4). Therefore, access to merozoites in the 45% of responses with detectable Ca^{2+}signals must have been through the activation of a diffusional path connecting RBC and merozoite compartments. To be able to elicit a saturated Ca^{2+}signal to emerge within a single frame transition of 0.1 s (Fig. 6 and Video S1), a high permeability pathway would have had to be generated soon after junction formation. Such a diffusional pathway would also allow other solutes to equilibrate across, Ca^{2+}ions among others. The spatial and temporal patterns of the $[Ca^{2+}]_i$ increase documented in the punctate responses (Fig. 6 and Video S1) are consistent with and support the view that a down-gradient flow of $Ca^{2+}$from merozoite to RBC can account for all the characteristics of the Ca^{2+}signals recorded from RBCs (Fig. 6).

Activation of the connecting pathway must have taken place in 45% of egress-invasion events regardless of whether or not Fluo-4 was there to visualize it. It may simply represent a premature or early formation of a membranous patch at the apical junction, precursor of the high permeability parasitophorous membrane (63–65) in a fraction of invasion events, of indifferent significance to its dynamic course. Alternatively, the connection may have evolved as a way of increasing invasion efficiency in selected RBC subpopulations. For instance, merozoites invading aging RBCs may activate early path formation to improve invasion efficiency, a point which future research may help resolve by investigating whether punctate-response frequencies vary in

a systematic way in age-segregated RBCs during invasion assays.

Together with the evidence that host calcium originated from the merozoite in the 45% of instances with punctate Ca^{2+}signals, the total absence of Ca^{2+}signals from Fluo-4-loaded RBCs in the 55% of Ca^{2+}-negative assays clearly argues against increases in the Ca^{2+}permeability of host RBCs during invasion and echinocytosis. Hence, the suggestion that rhoptries release factors that permeabilize host cells to Ca^{2+}secondarily triggering echinocytosis (10) is not supported by the available evidence. In addition, absence of late Ca^{2+}signals during the echinocytic stage, when the internalized parasite is surrounded by the parasitophorous vacuolar membrane, suggests that Fluo-4 diffusing from host cytoplasm towards the ring-stage parasite cannot access parasite domains of high-Ca^{2+}concentration any more.

4.2 On the mechanism of apical alignment

Demise of the calcium hypothesis rekindles the search for alternative mechanisms that could account for the dynamics of apical alignment. A few critical clues based on recent and earlier observations may be used to build a new coherent hypothesis amenable to theoretical and experimental tests. We can outline these clues as follows: i) only weak local deformations correlate with invasion efficiency (10, 12); ii) merozoite-host agonist-receptor interactions form reversible coat filaments of between about 20 to 150 nm in length capable of generating passive local membrane deformations on attachment and detachment (7, 66, 67); iii) certain agonist-receptor binding interactions (i.e EBA-175 and glycophorin A) activate signaling cascades that alter the physical properties of the host cell membrane priming it towards an increased invasion efficiency (19, 60); iv) the apex of the merozoite is positively charged relative to its base and to the negatively charged RBC surface (68); and v) apex-directed concentration gradients of agonists develop on the coat of activated merozoites (1, 12).

With these elements the dynamics of the pre-invasion stage leading to apical alignment may be envisaged as proceeding along the following sequence. Egress dispersal generates random and mostly apex-distant proximities between merozoites and target RBCs. When distances approach less than about 200 nm, agonist-receptor binding interactions (ARBIs) trigger the transient formation and contraction of "Bannister coat filaments, BCFs" (7) of long ($\sim$ 150 nm) and short ($\sim$ 20 nm) varieties, generating local bending deformations on target RBCs by passive compliance of the RBC membrane. The intensity of the effects caused by these transient adhesions will depend on the nature and surface density of ARBIs, on the bending modulus condition of the RBC membrane, and on the thermal and flickering fluctuations on its surface (69–72). The strength of each ARBI and associated BCF cluster is assumed to peak on formation and decay rapidly along an exponential time-course, thus allowing merozoites to detach and re-associate further with the same or other target RBCs. Crick *et al.* (67), observed that spent merozoites, with lost invasive capacity, attached irreversibly to RBCs as if the dissociation reaction had become blocked or inactivated, reminiscent of the condition of dehydrated RBCs surrounded by attached merozoites unable to invade (3). The irreversible attachment of spent merozoites offered the opportunity to measure the force of attachment. Using optical tweezers Crick *et al.* (67), calculated that a force of 40 ± 8 pN was needed to detach spent merozoites, probably near the peak force in a normal biphasic agonist-receptor binding reaction. Progress towards alignment will take place when successive merozoite attachments advance along the apex-directed agonist concentration gradient and electric field. Important modulating factors, with influence on apical alignment and invasion efficiency will be those affecting cytoskeletal tension and the viscoelastic and bending properties of the membrane (19, 60, 69, 72–74). These factors may be good candidates to account for the gradual decrease in invasion efficiency with increasing RBC density, because of the density-associated decrease in RBC deformability (75).

Essential components of the sequence just outlined as a mechanism of apical alignment were envisaged long ago by Bannister *et al.* (7), summarized in this quote from their paper: "Individual filaments are anchored to the membrane strongly enough to maintain attachment to red cells and to mediate considerable bending forces, although they allow re-orientation of the merozoite on the red cell, or even detachment, if effective apical contact is not made".

The passive compliance hypothesis of apical alignment outlined above can account for local deformations, but it offers no explanation for the large and distal dynamic deformations with which target RBCs often respond to merozoite contacts or proximities (4, 8). Without calcium mediation, the mechanism of these large deformation responses remains a challenging open question for future research.

Author Contribution VLL, PC and TT formulated the project and, together with VI designed the research; VI, AJC, TT, YCL cultured malaria parasites; VI, AJC and TT performed the experiments; JK developed the microscopy setup; VI processed and analysed the data; VI and VLL drafted the manuscript; PC and TT contributed in reviewing and editing the manuscript.

Acknowledgements We are grateful to Julian C. Rayner for providing 3D7 parasites and insightful comments. VI is funded by EPSRC, and Raymond and Beverly Sackler Foundation.

References

1. Cowman, A., and B. Crabb, 2006. Invasion of red blood cells by malaria parasites. *Cell* 124:755–766.

2. Koch, M., and J. Baum, 2016. The mechanics of malaria parasite invasion of the human erythrocyte - towards a reassessment of the host cell contribution. *Cellular Microbiology* 18:319–329.
3. Tiffert, T., 2005. The hydration state of human red blood cells and their susceptibility to invasion by *Plasmodium falciparum*. *Blood* 105:4853–4860.
4. Dvorak, J. A., L. H. Miller, W. C. Whitehouse, and T. Shiroishi, 1975. Invasion of erythrocytes by malaria merozoites. *Science* 187:748–750.
5. Lew, V., and T. Tiffert, 2007. Is invasion efficiency in malaria controlled by pre-invasion events? *Trends in Parasitology* 23:481–484.
6. Gilson, P., and B. Crabb, 2009. Morphology and kinetics of the three distinct phases of red blood cell invasion by *Plasmodium falciparum* merozoites. *International Journal for Parasitology* 39:91–96.
7. Bannister, L., G. Mitchell, G. Butcher, E. Dennis, and S. Cohen, 1986. Structure and development of the surface coat of erythrocytic merozoites of *Plasmodium knowlesi*. *Cell and Tissue Research* 245.
8. Glushakova, S., D. Yin, T. Li, and J. Zimmerberg, 2005. Membrane transformation during malaria parasite release from human red blood cells. *Current Biology* 15:1645–1650.
9. Crick, A. J., T. Tiffert, S. M. Shah, J. Kotar, V. L. Lew, and P. Cicuta, 2013. An automated live imaging platform for studying merozoite egress-invasion in malaria cultures. *Biophysical Journal* 104:997–1005.
10. Weiss, G. E., P. R. Gilson, T. Taechalertpaisarn, W.-H. Tham, N. W. M. de Jong, K. L. Harvey, F. J. I. Fowkes, P. N. Barlow, J. C. Rayner, G. J. Wright, A. F. Cowman, and B. S. Crabb, 2015. Revealing the sequence and resulting cellular morphology of receptor-ligand interactions during *Plasmodium falciparum* invasion of erythrocytes. *PLOS Pathogens* 11:1–25.
11. Tham, W.-H., N. Lim, G. Weiss, S. Lopaticki, B. Ansell, M. Bird, I. Lucet, D. Dorin-Semblat, C. Doerig, P. Gilson, B. Crabb, and A. Cowman, 2015. Plasmodium falciparum Adhesins Play an Essential Role in Signalling and Activation of Invasion into Human Erythrocytes. *PLOS Pathogens* 11:1–22.
12. Weiss, G., B. Crabb, and P. Gilson, 2016. Overlaying molecular and temporal aspects of malaria parasite invasion. *Trends in Parasitology* 32:284–295.
13. Treeck, M., S. Zacherl, S. Herrmann, A. Cabrera, M. Kono, N. Struck, K. Engelberg, S. Haase, F. Frischknecht, K. Miura, T. Spielmann, and T. Gilberger, 2009. Functional analysis of the leading malaria vaccine candidate AMA-1 reveals an essential role for the cytoplasmic domain in the invasion process. *PLoS Pathogens* 5:e1000322.
14. Crosnier, C., L. Bustamante, S. Bartholdson, A. Bei, M. Theron, M. Uchikawa, S. Mboup, O. Ndir, D. Kwiatkowski, M. Duraisingh, J. Rayner, and G. Wright, 2011. Basigin is a receptor essential for erythrocyte invasion by *Plasmodium falciparum*. *Nature* 480:534–537.
15. Mauritz, J., A. Esposito, H. Ginsburg, C. Kaminski, T. Tiffert, and V. Lew, 2009. The homeostasis of *Plasmodium falciparum*-infected red blood cells. *PLoS Computational Biology* 5:e1000339.
16. Waldecker, M., A. Dasanna, C. Lansche, M. Linke, S. Srismith, M. Cyrklaff, C. Sanchez, U. Schwarz, and M. Lanzer, 2017. Differential time-dependent volumetric and surface area changes and delayed induction of new permeation pathways in *P. falciparum*-infected hemoglobinopathic erythrocytes. *Cellular Microbiology* 19:e12650.
17. Wanaguru, M., W. Liu, B. Hahn, J. Rayner, and G. Wright, 2013. RH5-Basigin interaction plays a major role in the host tropism of *Plasmodium falciparum*. *Proceedings of the National Academy of Sciences* 110:20735–20740.
18. Wright, G., and J. Rayner, 2014. *Plasmodium falciparum* erythrocyte invasion: combining function with immune evasion. *PLoS Pathogens* 10:e1003943.
19. Koch, M., K. E. Wright, O. Otto, M. Herbig, N. D. Salinas, N. H. Tolia, T. J. Satchwell, J. Guck, N. J. Brooks, and J. Baum, 2017. *Plasmodium falciparum* erythrocyte-binding antigen 175 triggers a biophysical change in the red blood cell that facilitates invasion. *Proceedings of the National Academy of Sciences* 114:4225–4230.
20. Johnson, J., N. Epstein, T. Shiroishi, and L. Miller, 1980. Factors affecting the ability of isolated *Plasmodium knowlesi* merozoites to attach to and invade erythrocytes. *Parasitology* 80:539.
21. Wasserman, M., C. Alarcón, and P. Mendoza, 1982. Effects of Ca^{++} depletion on the asexual cell cycle of *Plasmodium Falciparum*. *The American Journal of Tropical Medicine and Hygiene* 31:711–717.
22. McCallum-Deighton, N., and A. Holder, 1992. The role of calcium in the invasion of human erythrocytes by *Plasmodium falciparum*. *Molecular and Biochemical Parasitology* 50:317–323.
23. Tsien, R., 1981. A non-disruptive technique for loading calcium buffers and indicators into cells. *Nature* 290:527–528.
24. Tsien, R., T. Pozzan, and T. Rink, 1982. T-cell mitogens cause early changes in cytoplasmic free Ca^{2+} and membrane potential in lymphocytes. *Nature* 295:68–71.
25. Tsien, R., 1982. Calcium homeostasis in intact lymphocytes: cytoplasmic free calcium monitored with a new, intracellularly trapped fluorescent indicator. *The Journal of Cell Biology* 94:325–334.
26. Lew, V., R. Tsien, C. Miner, and R. Bookchin, 1982. Physiological $[Ca^{2+}]_i$ level and pump-leak turnover in intact red cells measured using an incorporated Ca chelator. *Nature* 298:478–481.
27. Tsien, R., 1983. Intracellular measurements of ion activities. *Annual Review of Biophysics and Bioengineering* 12:91–116.
28. Tiffert, T., J. Garcia-Sancho, and V. L. Lew, 1984. Irreversible ATP depletion caused by low concentrations of formaldehyde and of calcium-chelator esters in intact human red cells. *Biochimica et Biophysica Acta (BBA) - Biomembranes* 773:143–156.
29. García-Sancho, J., 1985. Pyruvate prevents the ATP depletion caused by formaldehyde or calcium-chelator esters in the human red cell. *Biochimica et Biophysica Acta (BBA) - Biomembranes* 813:148–150.
30. Almaraz, L., and J. García-Sancho, 1989. Activation by calcium of AMP deaminase from the human red cell. *FEBS Letters* 244:417–420.
31. Dluzewski, A., K. Rangachari, R. Wilson, and W. Gratzer,

1983. A cytoplasmic requirement of red cells for invasion by malarial parasites. *Molecular and Biochemical Parasitology* 9:145–160.

32. Roberts, D., A. Craig, A. Berendt, R. Pinches, G. Nash, K. Marsh, and C. Newbold, 1992. Rapid switching to multiple antigenic and adhesive phenotypes in malaria. *Nature* 357:689–92.
33. Trager, W., and J. Jensen, 1976. Human malaria parasites in continuous culture. *Science* 193:673–675.
34. Tiffert, T., H. Ginsburg, M. Krugliak, B. C. Elford, and V. L. Lew, 2000. Potent antimalarial activity of clotrimazole in *in vitro* cultures of *Plasmodium falciparum*. *Proceedings of the National Academy of Sciences* 97:331–336.
35. Esposito, A., J. B. Choimet, J. N. Skepper, J. M. A. Mauritz, V. L. Lew, C. F. Kaminski, and T. Tiffert, 2010. Quantitative imaging of human red blood cells infected with *Plasmodium falciparum*. *Biophysical Journal* 99:953–960.
36. Lambros, C., and J. P. Vanderberg, 1979. Synchronization of *Plasmodium falciparum* erythrocytic stages in culture. *The Journal of Parasitology* 65:418.
37. Jensen, J. B., 1978. Concentration from continuous culture of erythrocytes infected with trophozoites and schizonts of *Plasmodium falciparum*. *The American Journal of Tropical Medicine and Hygiene* 27:1274–1276.
38. Pasvol, G., R. J. M. Wilson, M. E. Smalley, and J. Brown, 1978. Separation of viable schizont-infected red cells of *Plasmodium falciparum* from human blood. *Annals of Tropical Medicine & Parasitology* 72:87–88.
39. Coronado, L. M., N. M. Tayler, R. Correa, R. M. Giovani, and C. Spadafora, 2013. Separation of *Plasmodium falciparum* late stage-infected erythrocytes by magnetic means. *Journal of Visualized Experiments* .
40. Tiffert, T., H. M. Staines, J. C. Ellory, and V. L. Lew, 2000. Functional state of the plasma membrane Ca^{2+} pump in *Plasmodium falciparum*-infected human red blood cells. *The Journal of Physiology* 525:125–134.
41. García-Sancho, J., 1985. Pyruvate prevents the ATP depletion caused by formaldehyde or calcium-chelator esters in the human red cell. *Biochimica et Biophysica Acta (BBA) - Biomembranes* 813:148–150.
42. Lew, V., N. Daw, Z. Etzion, T. Tiffert, A. Muoma, L. Vanagas, and R. Bookchin, 2007. Effects of age-dependent membrane transport changes on the homeostasis of senescent human red blood cells. *Blood* 110:1334–1342.
43. Lew, V., N. Daw, D. Perdomo, Z. Etzion, R. Bookchin, and T. Tiffert, 2003. Distribution of plasma membrane Ca^{2+} pump activity in normal human red blood cells. *Blood* 102:4206–4213.
44. Tiffert, T., N. Daw, Z. Etzion, R. Bookchin, and V. Lew, 2007. Age decline in the activity of the $Ca2^{+}$-sensitive K^{+} channel of human red blood cells. *The Journal of General Physiology* 129:429–436.
45. Johnson, I., 2010. The molecular probes handbook: a guide to fluorescent probes and labeling technologies. Life Technologies Corporation, 11 edition.
46. Simonsen, L., J. Gomme, and V. Lew, 1982. Uniform ionophore A23187 distribution and cytoplasmic calcium buffering in intact human red cells. *Biochimica et Biophysica Acta (BBA) - Biomembranes* 692:431–440.
47. Tiffert, T., and V. Lew, 2001. Kinetics of inhibition of the plasma membrane calcium pump by vanadate in intact human red cells. *Cell Calcium* 30:337–342.
48. Lew, V., and H. Ferreira, 1978. Calcium transport and the properties of a calcium-activated potassium channel in red cell membranes. *In* Current Topics in Membranes and Transport, Elsevier, 217–277.
49. Gardos, G., 1958. The role of calcium in the potassium permeability of human erythrocytes. *Biochimica et Biophysica Acta* 30:653–654.
50. Litt, M., D. LaMorticella, C. Bond, and J. Adelman, 1999. Gene structure and chromosome mapping of the human small-conductance calcium-activated potassium channel SK1 gene (KCNN1). *Cytogenetic and Genome Research* 86:70–73.
51. Shah, M., and D. Haylett, 2000. The pharmacology of hSK1 Ca^{2+}-activated K^{+} channels expressed in mammalian cell lines. *British Journal of Pharmacology* 129:627–630.
52. Simons, T., 1976. Calcium-dependent potassium exchange in human red cell ghosts. *The Journal of Physiology* 256:227–244.
53. Lew, V., Z. Etzion, R. Bookchin, R. daCosta, H. Väänänen, M. Sassaroli, and J. Eisinger, 1993. The distribution of intracellular calcium chelator (fura-2) in a population of intact human red cells. *Biochimica et Biophysica Acta (BBA) - Biomembranes* 1148:152–156.
54. Begenisich, T., T. Nakamoto, C. Ovitt, K. Nehrke, C. Brugnara, S. Alper, and J. Melvin, 2004. Physiological roles of the intermediate conductance, Ca^{2+}-activated potassium channel Kcnn4. *Journal of Biological Chemistry* 279:47681–47687.
55. Hoffman, J., W. Joiner, K. Nehrke, O. Potapova, K. Foye, and A. Wickrema, 2003. The hSK4 (KCNN4) isoform is the Ca^{2+}-activated K^{+} channel (Gardos channel) in human red blood cells. *Proceedings of the National Academy of Sciences* 100:7366–7371.
56. Kirk, K., B. Elford, and J. Ellory, 1992. The increased K^{+} leak of malaria-infected erythrocytes is not via a Ca^{2+}-activated K^{+} channel. *Biochimica et Biophysica Acta (BBA)* 1135:8–12.
57. Staines, H., W. Chang, J. Ellory, T. Tiffert, K. Kirk, and V. Lew, 1999. Passive Ca^{2+} transport and Ca^{2+}-dependent K^{+} transport in Plasmodium falciparum-infected red cells. *Journal of Membrane Biology* 172:13–24.
58. Simons, T., 1982. A method for estimating free Ca within human red blood cells, with application to the study of their Ca-dependent K permeability. *Journal of Membrane Biology* 66:235–247.
59. Gao, X., K. Gunalan, S. Yap, and P. Preiser, 2013. Triggers of key calcium signals during erythrocyte invasion by *Plasmodium falciparum*. *Nature Communications* 4.
60. Sisquella, X., T. Nebl, J. K. Thompson, L. Whitehead, B. M. Malpede, N. D. Salinas, K. Rogers, N. H. Tolia, A. Fleig, J. O'Neill, W. Tham, F. D. David Horgen, and A. F. Cowman, 2017. *Plasmodium falciparum* ligand binding to erythrocytes induce alterations in deformability essential for invasion. *eLife* 6.
61. Aniweh, Y., X. Gao, P. Hao, W. Meng, S. Lai, K. Gunalan, T. Chu, A. Sinha, J. Lescar, R. Chandramohanadas, H. Li, S. Sze, and P. Preiser, 2017. *P. falciparum* RH5-Basigin interaction induces changes in the cytoskeleton of the host RBC. *Cellular Microbiology* 19:e12747.

62. Volz, J., A. Yap, X. Sisquella, J. Thompson, N. Lim, L. Whitehead, L. Chen, M. Lampe, W. Tham, D. Wilson, T. Nebl, D. Marapana, T. Triglia, W. Wong, K. Rogers, and A. Cowman, 2016. Essential role of the PfRh5/PfRipr/CyRPA complex during *Plasmodium falciparum* invasion of erythrocytes. *Cell Host & Microb* 20:60–71.
63. Bannister, L., and G. Mitchell, 2009. The malaria merozoite, forty years on. *Parasitology* 136:1435.
64. Dluzewski, A., D. Zicha, G. Dunn, and W. Gratzer, 1995. Origins of the parasitophorous vacuole membrane of the malaria parasite: surface area of the parasitized red cell. *European Journal of Cell Biology* 68:446–449.
65. Desai, S. A., and R. L. Rosenberg, 1997. Pore size of the malaria parasite′s nutrient channel. *Proceedings of the National Academy of Sciences* 94:2045–2049.
66. Bannister, L. H., G. H. Mitchell, G. A. Butcher, and E. D. Dennis, 1986. Lamellar membranes associated with rhoptries in erythrocytic merozoites of *Plasmodium knowlesi*: a clue to the mechanism of invasion. *Parasitology* 92:291–303.
67. Crick, A. J., M. Theron, T. Tiffert, V. L. Lew, P. Cicuta, and J. C. Rayner, 2014. Quantitation of malaria parasite-erythrocyte cell-cell interactions using optical tweezers. *Biophysical Journal* 107:846–853.
68. Aikawa, M., 1997. Studies on *falciparum* malaria with atomic-force and surface-potential microscopes. *Annals of Tropical Medicine & Parasitology* 91:689–692.
69. Yoon, Y., H. Hong, A. Brown, D. Kim, D. Kang, V. Lew, and P. Cicuta, 2009. Flickering analysis of erythrocyte mechanical properties: dependence on oxygenation level, cell shape, and hydration level. *Biophysical Journal* 97:1606–1615.
70. Fedosov, D., B. Caswell, and G. Karniadakis, 2010. Systematic coarse-graining of spectrin-level red blood cell models. *Computer Methods in Applied Mechanics and Engineering* 199:1937–1948.
71. Fedosov, D., B. Caswell, S. Suresh, and G. Karniadakis, 2010. Quantifying the biophysical characteristics of Plasmodium-falciparum-parasitized red blood cells in microcirculation. *Proceedings of the National Academy of Sciences* 108:35–39.
72. Dasgupta, S., T. Auth, N. S. Gov, T. Satchwell, E. Hanssen, E. Zuccala, D. Riglar, A. M. Toye, T. Betz, J. Baum, and G. Gompper, 2014. Membrane-wrapping contributions to malaria parasite invasion of the human erythrocyte. *Biophysical Journal* 107:43–54.
73. Fedosov, D., H. Lei, B. Caswell, S. Suresh, and G. Karniadakis, 2011. Multiscale Modeling of Red Blood Cell Mechanics and Blood Flow in Malaria. *PLoS Computational Biology* 7:e1002270.
74. Fedosov, D., M. Dao, G. Karniadakis, and S. Suresh, 2013. Computational Biorheology of Human Blood Flow in Health and Disease. *Annals of Biomedical Engineering* 42:368–387.
75. Suresh, S., 2006. Mechanical response of human red blood cells in health and disease: some structure-property-function relationships. *Journal of Materials Research* 21:1871–1877.